

# A Liquid Anode of Lithium Biphenyl for Highly Safe Lithium-Air Battery with Hybrid Electrolyte

Jiejun Bao,<sup>[a]</sup> Chao Li,<sup>[a]</sup> Fan Zhang,<sup>[a]</sup> Pengfei Wang,<sup>[a]</sup> Xueping Zhang,<sup>[a]</sup> Ping He,<sup>\*[a]</sup> and Haoshen Zhou<sup>\*[a, b]</sup>

A hybrid electrolyte, by uniting aqueous and organic electrolyte with a water-stable lithium super ionic conductor ceramic (LISICON) plate, was proposed to circumvent the drawbacks of nonaqueous Li-air batteries, such as corrosion of metallic Li from humidity, decomposition of organic solvents and insoluble discharge products clogging air electrode. However, safety issues deteriorate when the brittle ceramic plate fails to separate organic and aqueous solutions. This study aimed to improve the safety of the hybrid electrolyte based Li-air battery, by designing a liquid anode of lithium biphenyl (LiBP) replacing the lithium metal as the mild reaction between LiBP and aqueous electrolyte without combustion. Moreover, sputtering Ti layer onto the anodic side of the ceramic plate can improve chemical stability of interface between the liquid anode and solid electrolyte. In this system, the cell exhibited a relatively high discharge voltage of 2.81 V at the current density of 0.5 mA cm<sup>-2</sup>, as well as a specific power of 1638 W kg<sup>-1</sup> at the current density of 6 mA cm<sup>-2</sup> by using this liquid anode. The cycling life exceeded over 120 cycles at the current density of 0.5 mA cm<sup>-2</sup>. The *ex situ* Raman spectrometry and *in situ* GC-MS analyses reveal that the redox reaction of BP<sup>-</sup>/BP and OH<sup>-</sup>/O<sub>2</sub> in anolyte and catholyte respectively can deliver large capacity during cycling.

Although rechargeable Li-ion batteries have been extensively used in electric vehicles (EVs), their energy density remains insufficient to meet the rapid development of long-range EVs.<sup>[1]</sup> Unlike conventional Li-ion batteries, Li-air batteries deliver capacity by reducing O<sub>2</sub> from air. Thus, the energy density of Li-air battery is much higher than that of conventional Li-ion battery. The Li-air batteries with a polymer electrolyte, were first reported in 1996.<sup>[2]</sup> Following this study, several research

groups have focused on the nonaqueous Li-air battery, with the structure of Li|organic electrolyte|air electrode.<sup>[3]</sup> According to the reaction  $2\text{Li} + \text{O}_2 \rightarrow \text{Li}_2\text{O}_2$ , the theoretical specific energy is 3600 Wh kg<sup>-1</sup> for Li-air battery. However, the nonaqueous Li-air battery still suffers from some serious problems, i.e., O<sub>2</sub>, CO<sub>2</sub> and H<sub>2</sub>O from air dissolving in organic electrolyte can directly react with metallic Li;<sup>[4]</sup> Some oxidizing intermediates such as LiO<sub>2</sub>, O<sub>2</sub><sup>2-</sup> or singlet oxygen <sup>1</sup>O<sub>2</sub> may attack the organic solvent;<sup>[5]</sup> the discharge product Li<sub>2</sub>O<sub>2</sub> is insoluble in organic electrolyte and thus gradually clogs the porous air cathode.<sup>[6]</sup>

Zhou and Wang firstly reported a new type of Li-air battery with a hybrid electrolyte to overcome the drawbacks of nonaqueous Li-air battery.<sup>[7]</sup> In the hybrid electrolyte system, the organic anolyte and aqueous catholyte are separated by a ceramic LISICON plate as solid Li<sup>+</sup> conducting electrolyte. Given that the O<sub>2</sub> reduction product is soluble in aqueous catholyte, the clogging issue in the porous air cathode can be avoided.<sup>[8]</sup> However, several challenges in using metallic Li anode still remain to be solved in the hybrid system. For example, the Columbic efficiency is poor because of the irreversible Li striping/plating and parasitic reactions between metallic Li and organic electrolyte.<sup>[9]</sup> Many strategies have been devoted to solving this problem, such as the introduction of additives into electrolyte<sup>[10]</sup> and the design of a 3D lithophilic current collector.<sup>[11]</sup> These efforts have improved the Columbic efficiency of metallic Li. Nevertheless, few works noticed the concern on safety existing in the hybrid system. The brittle solid electrolyte plate, which plays the important role of high conducting solid electrolyte, is bound to pose safety hazards when it cracks gradually during discharging and charging.<sup>[12]</sup> The failure of separating organic and aqueous electrolytes can result in drastic reactions between metallic Li and aqueous solution from the catholyte. Indeed, safety issues in hybrid electrolyte based Li-air batteries need to be addressed urgently.

In 2017, Hu et al.<sup>[13]</sup> reported a liquid anode of sodium biphenyl solution for Na–S battery. Their work improved the efficiency of the metallic sodium anode and the battery's safety. The reactions between sodium biphenyl and bulk water proceeded mildly without combustion. After that, Lu et al.<sup>[14]</sup> used analogous potassium biphenyl solution as anode for nonaqueous K–O<sub>2</sub> battery with long life and low-level hazard. Based on these reports, the biphenyl complex solution exhibits a low redox potential and high safety. Thus, by using the lithium biphenyl (hereafter denoted as LiBP) solution as anode,

[a] J. Bao, C. Li, F. Zhang, P. Wang, X. Zhang, Prof. P. He, Prof. H. Zhou  
Center of Energy Storage Materials & Technology  
College of Engineering and Applied Sciences  
Jiangsu Key Laboratory of Artificial Functional Materials  
National Laboratory of Solid State Microstructures, Collaborative Innovation  
Center of Advanced Microstructures  
Nanjing University, Nanjing 210093, PR China  
E-mail: pinghe@nju.edu.cn  
hszhou@nju.edu.cn

[b] Prof. H. Zhou  
Prof. H. S. Zhou  
Energy Technology Research Institute  
National Institute of Advanced Industrial Science and Technology (AIST)  
Tsukuba, Japan

 Supporting information for this article is available on the WWW under  
<https://doi.org/10.1002/batt.202000092>

the safety of hybrid electrolyte based Li-air battery can be improved.

Herein, analogous lithium biphenyl solution was introduced into the hybrid electrolyte based Li-air battery as the liquid anode to solve the safety problems (Figure 1a). The catalyst used was a Pt/C composite and the catholyte was an aqueous solution of  $\text{Li}_2\text{SO}_4$ . The NASICON-type solid electrolyte  $\text{Li}_{1.5}\text{Al}_{0.5}\text{Ge}_{1.5}(\text{PO}_4)_3$  (LAGP) was used to separate the liquid LiBP anode and catholyte. The solid electrolyte LAGP was synthesized through a conventional solid-state reaction according to our previous work.<sup>[15]</sup> The SEM and optical images of the LAGP plate are shown in Figure S1a. The diffraction peaks of LAGP plate corresponding to the NASICON-structured  $\text{LiGe}_2(\text{PO}_4)_3$  phase were observed in Figure S1d, and these peaks can be attributed to the similar ionic radii of  $\text{Ge}^{4+}$  and  $\text{Al}^{3+}$ . The LAGP plate also was confirmed by the Rietveld refinement of the XRD pattern in Figure S2. The total lithium ionic conductivity of the ceramic LAGP was calculated to be  $1.40 \times 10^{-4} \text{ S cm}^{-1}$  based on electrochemical impedance spectroscopy (EIS) test in Figure S1b.

The liquid LiBP anode was prepared by simply dissolving metallic Li into a solution of biphenyl in dimethoxyethane. A dark blue solution was obtained as shown in Figure S1c. The reaction between metallic Li and water is known to be very violent. To verify the safety of the prepared liquid LiBP anode with aqueous solution, different volumes of aqueous solution were added into the LiBP as shown in Figure 1b. When 50  $\mu\text{L}$  aqueous solution was added, the color of liquid LiBP changed slightly. Even when 500  $\mu\text{L}$  solution was added, the separation

between aqueous and LiBP solutions caused the reaction to be very mild. We also added the aqueous solution into the liquid LiBP dropwise, as shown in the Supplementary Video. These results indicated that the reaction between LiBP and aqueous solution was gentler than that of metallic Li. Thus, safety level of liquid LiBP toward aqueous solution is much higher than that of metallic Li.

The liquid LiBP anode was characterized by the Raman spectroscopy. As shown in the Raman patterns in Figure 2a, biphenyl radical anion existed in solution.<sup>[16]</sup> The redox behavior of the LiBP was characterized by cyclic voltammetry tests, and the results are shown in Figure 2b. The redox potential ( $E_{1/2}$ ) is about 0.30 V versus  $\text{Li}/\text{Li}^+$ . Apparently, the liquid LiBP anode can undergo reversible redox reaction and its redox potential is sufficiently low that it could be an alternative to Li anode. Combined with an air cathode, the hybrid Li-air battery using this liquid anode could achieve a high cell voltage as shown in Figure 2b and Figure S3a. For the conductivity of the liquid LiBP anode, Zhou reported that it improved with the increase of LiBP concentration and the conductivity was calculated to be  $1.11 \times 10^{-2} \text{ S cm}^{-1}$  at the concentration of 1 M. So, these values are sufficient for an electrode application.<sup>[17]</sup> Thus, the  $\text{LiBP}|\text{LAGP}|\text{Pt/C}$  cell was assembled and placed in ambient air for 2 h. And Figure S3b shows that the open-circuit voltage (OCV) of the cell is 3.41 V.

The electrochemical reactions of the liquid LiBP anode and the air cathode were investigated by *ex situ* Raman spectrometry and *in situ* gas chromatography-mass spectrometry (GC-MS), respectively. We obtained the *ex situ* Raman spectra of the liquid anode at various states, as shown in Figure 2c and Figure S5. In pristine state, the Raman patterns at 979, 1017, 1326 and 1587  $\text{cm}^{-1}$  are assigned to signals of biphenyl radical anion ( $\text{BP}^-$ ). After discharging to 1.5 V, the above Raman patterns shift to 1005, 1033, 1287 and 1613  $\text{cm}^{-1}$ , and the peak

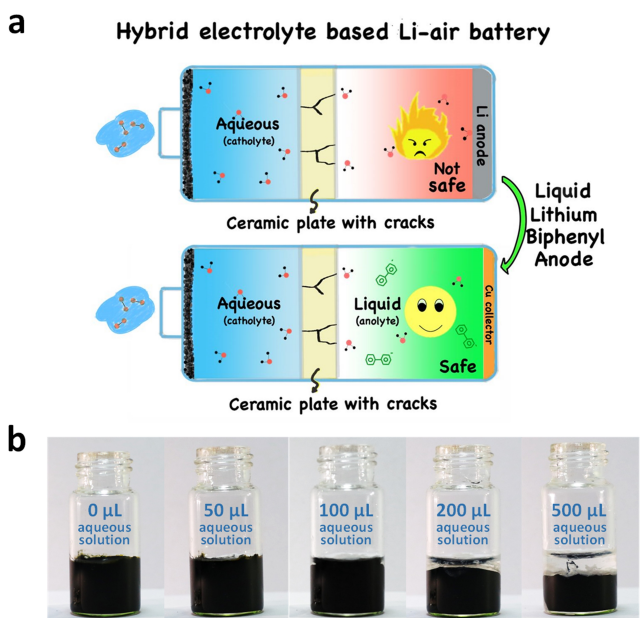


**Figure 1.** a) Schematic of the hybrid electrolyte based Li-air batteries with different anodes in case of ceramic plate breaking under harsh operational and abuse conditions. Water from the aqueous catholyte reacts with metallic Li and liquid lithium biphenyl anode respectively. Liquid lithium biphenyl anode is employed to be an alternative to metallic Li to improve the safety as the mild reaction with water. b) Safety measurement: adding different volumes of 0.5 M  $\text{Li}_2\text{SO}_4$  solution (0, 50, 100, 200, 500  $\mu\text{L}$ ) into liquid LiBP.

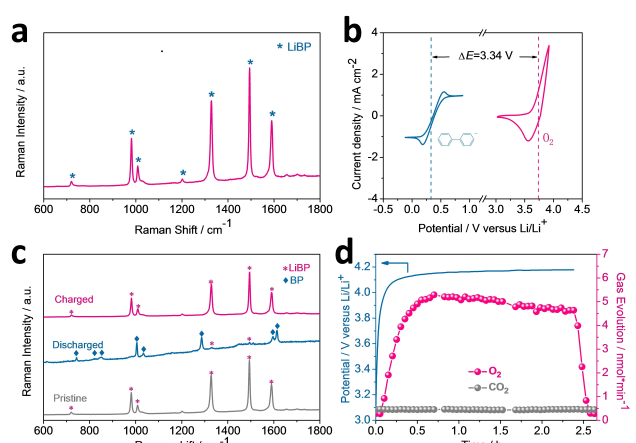
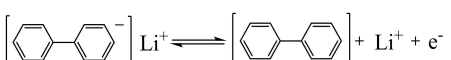


**Figure 2.** a) Raman spectra of LiBP. b) CV curves of 10 mM BP (blue) in 0.5 M  $\text{LiPF}_6$  in 1,2-dimethoxyethane(DME) and saturated  $\text{O}_2$  in 0.5 M  $\text{Li}_2\text{SO}_4$  solution (rose red) on a glass carbon electrode at 50  $\text{mVs}^{-1}$ ; Pt wire both was used as the counter electrode. c) *Ex situ* Raman spectra of the liquid anode shown at different states: pristine (grey), discharged (red) and charged (blue) state. d) GC-MS profiles of the air cathode during the charge process: galvanostatic charge voltage (blue) and gas evolution including  $\text{O}_2$  (red) and  $\text{CO}_2$  (grey) at the current density of  $0.5 \text{ mA cm}^{-2}$ .

at  $1493\text{ cm}^{-1}$  vanishes, corresponding to signals of biphenyl (BP). It suggests that  $\text{BP}^-$  transformed into BP in the liquid anode during discharge. When charging to 4.5 V, the Raman patterns of  $\text{BP}^-$  are observed again. Based on the above results, the electrochemical reaction of the liquid LiBP anode is a reversible reaction between  $\text{BP}^-$  and BP during discharge and charge. Furthermore, GC-MS was used to study the reaction of the air cathode during the charge process at the current density of  $0.5\text{ mA cm}^{-2}$ . The gas-evolution rate and the corresponding charge voltage are exhibited in Figure 2d. The tendency of the  $\text{O}_2$  evolution rate is synchronized with the charge process and no  $\text{O}_2$  was detected after cell resting. Meanwhile, no  $\text{CO}_2$  and other gases were generated throughout the entire process. Thus, the electrode reactions are as follows:

Anode:



Cathode:



Figure 3 shows the electrochemical performances of the cell based on liquid LiBP anode. The galvanostatic discharge profiles at different current densities ranging within  $0.01\text{--}10\text{ mA cm}^{-2}$  are presented in Figure 3a. The voltage lies at  $3.32\text{ V}$  at the current density of  $0.01\text{ mA cm}^{-2}$ , and this value is close to the OCV. Even at the current density of  $3\text{ mA cm}^{-2}$ , the voltage is still  $2.16\text{ V}$ . The operating voltage decreases linearly with increased applied current density (Figure 3a). From the current-voltage curve, the inner resistance was estimated to be the resistance of the solid electrolyte LAGP.<sup>[18]</sup> The power-generation test was carried out and the results are also shown

in Figure 3b. The specific power of the cell was calculated according to the mass of the catalyst layer. The maximum specific power reached  $1638\text{ W kg}^{-1}$  at a high discharge current density of  $6\text{ mA cm}^{-2}$ . Remarkably, the liquid anode can reach a very high concentration in DME solvent, so we can improve the specific capacity by using the liquid anode with a high concentration.<sup>[19]</sup> The full discharge-charge processes of the cell based on liquid anode with different concentrations at the current density of  $1\text{ mA cm}^{-2}$  were compared, and the results are shown in Figure 3c. The specific capacity of the cell with  $1\text{ M}$  liquid-anode concentration is  $3036\text{ mAh g}^{-1}$  based on the catalyst-layer mass. With increasing concentration to  $3\text{ M}$ , the specific capacity increases threefold to  $9244\text{ mAh g}^{-1}$ .

The cycling performance of the cell based on liquid  $1\text{ M}$  LiBP anode was investigated by galvanostatic discharge-charge tests at the current density of  $0.5\text{ mA cm}^{-2}$  with a limited areal capacity of  $1\text{ mAh cm}^{-2}$  (Figure 3d). The cell displays a relatively high discharge voltage of  $2.81\text{ V}$  in the first cycle. However, the voltage plateau declines to  $2.07\text{ V}$  after 30 cycles. As shown in Figure S6, the discharge and charge overpotential of the cell increased with prolonged cycling time, and the cell failed after 45 cycles. We also examined the cycling performance of the cell with high concentration of LiBP anode in Figure S7. The cell with  $3\text{ M}$  LiBP anode has a worse stability than  $1\text{ M}$  LiBP | LAGP | Pt/C cell and the discharge voltage plateau drops to  $1.79\text{ V}$  after 11 cycles. This failure of the cell is possibly caused by the side reactions between the solid electrolyte LAGP and liquid anode. Details of the side reactions are discussed below.

Given the low reductive potential ( $0.3\text{ V}$  vs.  $\text{Li}/\text{Li}^+$ ) of the liquid LiBP anode,  $\text{Ge}^{4+}$  in LAGP will be reduced, leading to the rapid degradation of batteries.<sup>[20]</sup> Some black products were generated on the anodic side of LAGP plate (Figure S8a). The reactions between LAGP powder and LiBP solution were investigated by X-ray photoelectron spectroscopy and Raman spectroscopy. The  $\text{Ge}$  3d line for the pristine material at  $32.3\text{ eV}$  well matches the binding energy values of  $\text{Ge}^{4+}$ . After immersion in liquid LiBP for 2 h, two new lines at  $31.2$  and  $29.2\text{ eV}$  are detected, and they can be attributed to Ge of lower oxidation states (Figure S9). Additionally, some peaks of BP appear in the Raman spectra of LiBP after reaction (Figure S8b). These results clearly suggest the LAGP can be reduced by the liquid LiBP anode. The side reactions lead to the increase of interfacial resistance and the degradation of the liquid anode.

To enhance the chemical stability of ceramic LAGP plate in liquid LiBP anode, a thin coating layer could be sputtered on the anodic side of LAGP plate to protect the solid electrolyte.<sup>[21]</sup> The thin coating layer should be stable in liquid LiBP. Titanium (Ti) exhibits high resistance against corrosion and thus has extensive biomedical and dental applications.<sup>[22]</sup> To investigate the stability of Ti in LiBP solution, a Ti plate was immersed in the liquid LiBP anode for 2 weeks. The XRD of the Ti plate and the Raman spectra of the LiBP remain unchanged, as shown in Figure S10. Thus, a Ti coating layer can be formed on LAGP plate (Ti-LAGP) by DC magnetron sputtering to protect the solid electrolyte in this work. To obtain the appropriate sputtering time of the Ti-LAGP, we investigated the relationship between Ti sputtering time and electrochemical proper-

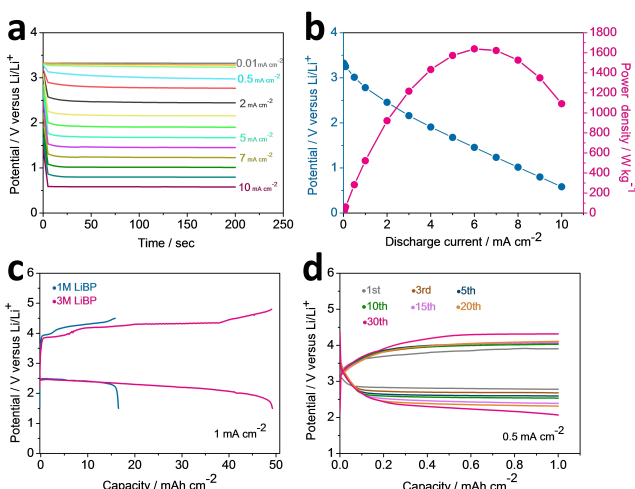


**Figure 3.** The electrochemical characterization of the  $1\text{ M}$  LiBP | LAGP | Pt/C cell. a) The galvanostatic discharge profiles at different current densities ranging within  $0.01\text{--}10\text{ mA cm}^{-2}$ . b) The current-voltage and the specific power-voltage profiles. c) The full discharge-charge profiles of LiBP | LAGP | Pt/C cell with  $1\text{ M}$  and  $3\text{ M}$  LiBP solution at the current density of  $1\text{ mA cm}^{-2}$ . d) The discharge-charge profiles at the current density of  $0.5\text{ mA cm}^{-2}$  with a limited areal capacity of  $1\text{ mAh cm}^{-2}$ .

ties. As the results of the electrochemical impedance spectroscopy of the LAGP with different Ti sputtering time shown in Figure S11a, the appropriate sputtering time of the Ti protective layer is 10 min with a comparatively high conductivity of  $1.02 \times 10^{-4} \text{ S cm}^{-1}$ . The Ti-LAGP also has less effects on the electrochemical performance with 10 min sputtering time in the Figure S11b. Thus, the appropriate sputtering time of the Ti protective layer is 10 min.

After sputtering for 10 min, the color of LAGP changed from white to gray, as shown in Figure S12a. The SEM images show that the Ti-coated LAGP plate had a smoother surface than the initial LAGP surface with micro-sized LAGP grains (Figure S12b). Figure 4a shows the cross-sectional SEM of Ti-LAGP plate. A thin Ti-coating layer about 300 nm was uniformly deposited on the surface. EDS mapping further confirmed the successful deposition of Ti layer, as shown in Figure 4b. The stability test of the LAGP and Ti-LAGP with LiBP anode was verified in Figure S13. When adding a drop of LiBP on the surface of LAGP and Ti-LAGP, the surface of LAGP facing the LiBP became black after one week. By contrast, the surface of Ti-LAGP had no obvious change in the color.

The LiBP|Ti-LAGP|Pt/C cell was assembled to test its cycling performance. Figure 4c shows the discharge-charge profiles at the current density of  $0.5 \text{ mA cm}^{-2}$  with a limited

areal capacity of  $1 \text{ mAh cm}^{-2}$ . The first discharge voltage is about 2.65 V, which is lower than that of the cell without Ti layer because an extra Ti layer was introduced into the cell with lower  $\text{Li}^+$  conductivity.<sup>[23]</sup> However, the cycling life of the cell with protective Ti layer at  $0.5 \text{ mA cm}^{-2}$  having a limited areal capacity of  $1 \text{ mAh cm}^{-2}$  can exceed over 120 cycles, which is extremely longer than the cell without Ti layer (Figure 4c). EIS analysis of the cells with and without Ti protective layer was performed before and after cycling. For the cell without Ti layer, the impedance changed greatly after 50 cycles. It can be seen that the ohmic resistance ( $R_{\text{e}}$ ) of the cell increases from 276.4 to  $861.6 \Omega$  in Figure 4d. The high-frequency semicircle (related to the grain boundary in the LAGP plate and porous air electrode) also increases after cycling. By contrast, the impedance of the cell with Ti layer changed slightly after 100 cycles in Figure 4e. As shown in Figure S14, the Ti protective layer also improved the cycling performance of 3 M LiBP|Ti-LAGP|Pt/C cell. This performance improvement is attributed to the protective Ti layer alleviating the side-reaction rate between LAGP and liquid anode.

In conclusion, liquid LiBP anode was applied in Li-air batteries based on hybrid electrolyte to improve the safety of this system and we further enhanced the cycling performance of the cell with LiBP anode through sputtering Ti protective layer. LiBP was used as the liquid anode to decrease the hazard level, because of its gentle reaction with aqueous solution. The hybrid Li-air battery with LiBP anode exhibited a relatively high discharge voltage of 2.81 V at the current density of  $0.5 \text{ mA cm}^{-2}$ , as well as a specific power of  $1638 \text{ W kg}^{-1}$  at the current density of  $6 \text{ mA cm}^{-2}$ . High-concentration LiBP was used as the anode to improve specific capacity. With increasing concentration of liquid LiBP anode to 3 M, the specific capacity is about  $9244 \text{ mAh g}^{-1}$ . Besides, after sputtering a thin Ti layer on the anodic side of LAGP plate, the cycling life was enhanced because the Ti protective layer can prevent the side reactions between LAGP and the liquid anode. The cell with protective Ti layer can operate over 120 cycles. The *ex situ* Raman spectrometry and *in situ* GC-MS analyses reveal that the redox reaction of  $\text{BP}^-/\text{BP}$  and  $\text{OH}^-/\text{O}_2$  in anolyte and catholyte respectively can deliver large capacity during cycling.

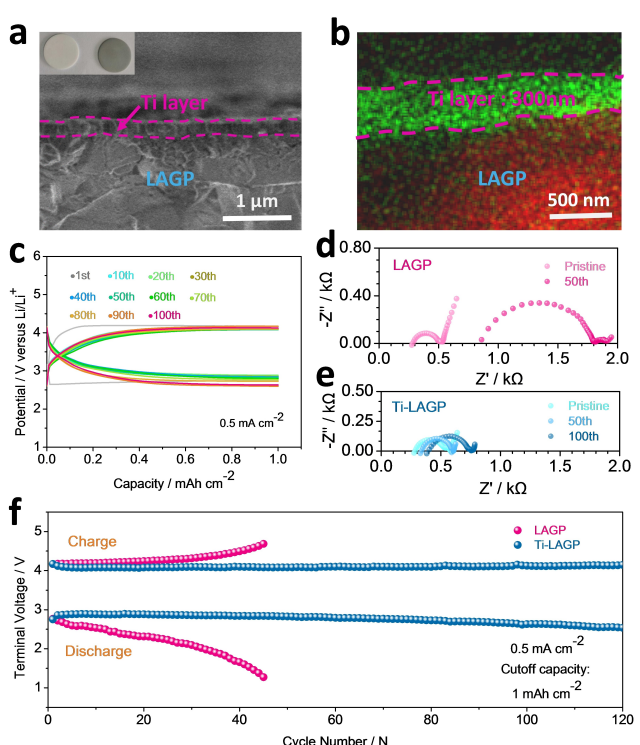


**Figure 4.** a) The cross-sectional SEM images of Ti-LAGP plate with inset showing the optical images. b) EDS-mapping of the side view of the Ti-LAGP plate. c) The discharge-charge profiles of 1 M LiBP|Ti-LAGP|Pt/C cell at the current density of  $0.5 \text{ mA cm}^{-2}$  with a limited areal capacity of  $1 \text{ mAh cm}^{-2}$ . d) The electrochemical impedance spectroscopy of 1 M LiBP|LAGP|Pt/C and e) 1 M LiBP|Ti-LAGP|Pt/C cell before and after cycling. f) The terminal voltage-cycles of the 1 M LiBP|Ti-LAGP|Pt/C and 1 M LiBP|LAGP|Pt/C cell at the current density of  $0.5 \text{ mA cm}^{-2}$  with a limited areal capacity of  $1 \text{ mAh cm}^{-2}$ .

## Acknowledgements

This research was partially supported by the National Key Research and Development Program of China (2016YFB0100203), the National Natural Science Foundation of China (21922508, 21673116, 21633003 and U1801251), the Fundamental Research Funds for the Central Universities (021314380176), the Natural Science Foundation of Jiangsu Province (BK20190009), and PAPD of Jiangsu Higher Education Institutions.

## Conflict of Interest

The authors declare no conflict of interest.

**Keywords:** hybrid electrolyte • Li-air battery • liquid lithium biphenyl • high safety • Ti protective layer

- [1] P. G. Bruce, S. A. Freunberger, L. J. Hardwick, J. M. Tarascon, *Nat. Mater.* **2011**, *11*, 19–29.
- [2] K. Abraham, Z. Jiang, *J. Electrochem. Soc.* **1996**, *143*, 1–5.
- [3] a) T. Ogasawara, A. Débart, M. Holzapfel, P. Novák, P. G. Bruce, *J. Am. Chem. Soc.* **2006**, *128*, 1390–1393; b) Z. Peng, S. A. Freunberger, Y. Chen, P. G. Bruce, *Science*, **2012**, *337*, 563–566.
- [4] Z. Guo, X. Dong, S. Yuan, Y. Wang, Y. Xia, *J. Power Sources* **2014**, *264*, 1–7.
- [5] L. Johnson, C. Li, Z. Liu, Y. Chen, S. A. Freunberger, P. C. Ashok, B. B. Praveen, K. Dholakia, J. M. Tarascon, P. G. Bruce, *Nat. Chem.* **2014**, *6*, 1091.
- [6] F. Cheng, J. Chen, *Chem. Soc. Rev.* **2012**, *41*, 2172–2192.
- [7] Y. Wang, H. Zhou, *J. Power Sources* **2010**, *195*, 358–361.
- [8] a) Y. Wang, P. He, H. Zhou, *Energy Environ. Sci.* **2011**, *4*, 4994–4999; b) P. He, Y. Wang, H. Zhou, *Electrochim. Commun.* **2010**, *12*, 1686–1689.
- [9] a) W. Xu, J. Wang, F. Ding, X. Chen, E. Nasybulin, Y. Zhang, J. G. Zhang, *Energy Environ. Sci.* **2014**, *7*, 513–537; b) Y. Ding, G. Yu, *Angew. Chem. Int. Ed.* **2016**, *55*, 4772–4776; *Angew. Chem.* **2016**, *128*, 4850–4854.
- [10] a) X. Q. Zhang, X. B. Cheng, X. Chen, C. Yan, Q. Zhang, *Adv. Funct. Mater.* **2017**, *27*, 1605989; b) X. Q. Zhang, X. Chen, X. B. Cheng, B. Q. Li, X. Shen, C. Yan, J. Q. Huang, Q. Zhang, *Angew. Chem. Int. Ed.* **2018**, *57*, 5301–5305; *Angew. Chem.* **2018**, *130*, 5399–5403.
- [11] a) C. Zhang, S. Liu, G. Li, C. Zhang, X. Liu, J. Luo, *Adv. Mater.* **2018**, *30*, 1801328; b) X. Zhang, R. Lv, A. Wang, W. Guo, X. Liu, J. Luo, *Angew. Chem. Int. Ed.* **2018**, *57*, 15028–15033.
- [12] a) S. Zekoll, C. Marriner Edwards, A. K. O. Hekselman, J. Kasemchainan, C. Kuss, D. E. J. Armstrong, D. Cai, R. J. Wallace, F. H. Richter, J. H. J. Thijssen, P. G. Bruce, *Energy Environ. Sci.* **2018**, *11*, 185–201; b) H. Xie, Y. Bao, J. Cheng, C. Wang, E. M. Hitz, C. Yang, Z. Liang, Y. Zhou, S. He, T. Li, *ACS Energy Lett.* **2019**, *4*, 2668–2674.
- [13] J. Yu, Y. S. Hu, F. Pan, Z. Zhang, Q. Wang, H. Li, X. Huang, L. Chen, *Nat. Commun.* **2017**, *8*, 14629.
- [14] G. Cong, W. Wang, N. C. Lai, Z. Liang, Y. C. Lu, *Nat. Mater.* **2019**, *18*, 390–396.
- [15] Y. Liu, B. Li, Z. Cheng, C. Li, X. Zhang, S. Guo, P. He, H. Zhou, *J. Power Sources* **2018**, *395*, 439–443.
- [16] C. Takahashi, S. Maeda, *Chem. Phys. Lett.* **1974**, *24*, 584–588.
- [17] H. Deng, Z. Chang, F. Qiu, Y. Qiao, H. Yang, P. He, H. Zhou, *Adv. Energy Mater.* **2020**, *10*.1002/aenm.201903953.
- [18] Z. Li, M. S. Pan, L. Su, P. C. Tsai, A. F. Badel, J. M. Valle, S. L. Eiler, K. Xiang, F. R. Brushett, Y. M. Chiang, *Joule* **2017**, *1*, 306–327.
- [19] F. Liang, X. Qiu, Q. Zhang, Y. Kang, A. Koo, K. Hayashi, K. Chen, D. Xue, K. N. Hui, H. Yadegari, X. Sun, *Nano Energy* **2018**, *49*, 574–579.
- [20] F. Pan, J. Yang, C. Jia, H. Li, Q. Wang, *J. Energy Chem.* **2018**, *27*, 1362–1368.
- [21] Y. Liu, C. Li, B. Li, H. Song, Z. Cheng, M. Chen, P. He, H. Zhou, *Adv. Energy Mater.* **2018**, *8*, 1702374.
- [22] F. Trevisan, F. Calignano, A. Aversa, G. Marchese, M. Lombardi, S. Biamino, D. Ugues, D. Manfredi, *J. Appl. Biomater. Funct. Mater.* **2017**, *16*, 57–67.
- [23] H. Lee, X. Ren, C. Niu, L. Yu, M. H. Engelhard, I. Cho, M. H. Ryou, H. S. Jin, H. T. Kim, J. Liu, *Adv. Funct. Mater.* **2017**, *27*, 1704391.

Manuscript received: April 24, 2020

Accepted manuscript online: May 7, 2020

Version of record online: May 25, 2020